 doi:10.20944/preprints202205.0183.v1

Article

Full-scale demonstration of combined ground source heating and sustainable urban drainage in roadbeds

Søren Erbs Poulsen [1]*, Theis Raaschou Andersen [1] and Karl Woldum Tordrup [1]

[1] VIA University College, R&D Centre for the Built Environment, Energy, Water and Climate
* Correspondence: soeb@via.dk; Tel.: +45 87554209

Abstract: This paper proposes and demonstrates, in full scale, a novel type of energy geostructure ("the Climate Road") that combines a ground source heat pump (GSHP) with a sustainable urban drainage system (SUDS) by utilizing the gravel roadbed simultaneously as energy source and rainwater retarding basin. The Climate Road measures 50m x 8m x 1m (length, width, depth) and has 800 m of geothermal piping embedded in the roadbed, serving as the heat collector for a GSHP that supplies a nearby kindergarten with domestic hot water and space heating. Model analysis of operational data from 2018-2021 indicates sustainable annual heat production levels around 0.6 MWh per meter road, with a COP of 2.9-3.1. The continued infiltration of rainwater to the roadbed increases the amount of extractable heat by an estimated 17% compared to the case of zero infiltration. Using the developed model for scenario analysis we find that draining rainwater from three single family houses and storing 30% of the annual heating consumption in the roadbed, increases the predicted extractable energy by 56% compared to zero infiltration with no seasonal energy storage. The Climate Road is capable of supplying three single family houses with heating, cooling and rainwater management year-round.

Keywords: Energy geostructure; ground source heat pump (GSHP); sustainable urban drainage system (SUDS); sector integration; 5th generation district heating and cooling; permeable asphalt; rainwater retardation; full-scale demonstration; numerical modelling; analytical modelling

1. Introduction

The IPCC report from 2022 predicts catastrophic and irreversible climate change unless immediate and sustained reductions in emissions of carbon dioxide and other greenhouse gases are enforced on a global scale [1]. The heating and cooling sector consumes as much as 50% of the total final energy use in Europe and its decarbonization, by implementing renewable energy sources, has become even more urgent [2]. Geothermal energy is both clean and renewable and is expected to play a major role in the decarbonization of the global energy sector [3]. The installed capacity of geothermal heat pumps has increased by 70% from 2015 to 2020 indicating a rapidly growing market for geothermal energy [4]. Ground source heat pumps (GSHP) are efficient relative to air source heat pumps (ASHP) and are also able to supply direct/passive cooling due to the constant and low temperature of the ground [5-8]. The utilization of shallow geothermal energy has gained further interest with the emergence of 5th generation district heating and cooling (5GDHC) grids with distributed ground source heat pumps that extract and store energy in the shallow subsurface typically between 0 and 200 m depth [9-11]. The introduction of 5GDHC exemplifies successful integration in the energy sector, by advancing direct electrification of prosumer-based circular, efficient and renewable heating and cooling grids, and constitutes one of several promising strategies to address the pressing issue of climate change [11]. Integration across different sectors such as groundwater, heating and cooling, electricity, wastewater etc. by means of multifunctional supply and utility systems, potentially holds further efficiency gains and decarbonization possibilities [12,13].

 doi:10.20944/preprints202205.0183.v1

The increasing urbanization of the global population limits the available urban space for utility infrastructure. Price et al. developed a 3D engineering geological model to maximize the use of the subsurface for sustainable urban drainage and ground source heating while screening the foundation potential [14]. They consider energy geostructures which embed energy collectors for GSHPs in structural building elements and thus exemplify integration of the building and energy sectors by creating added value from economies of scope, as the need for structural building elements facilitates cost-effective heating and cooling. In previous work, we have studied the use of foundation pile heat exchangers (energy piles) as the main energy source for a 5GDHC grid in Vejle, Denmark [15]. We estimated a payback period of 4-7 years for the energy pile-based 5GDHC grid relative to traditional district heating largely due to the significant cost reduction for the ground heat exchangers and greatly reduced variable costs. Several other types of energy geostructures have been successfully developed and implemented including energy walls, tunnels, and ground anchors [16-18]. Charlesworth et al. embedded GSHP geothermal piping in a permeable pavement system (PPS) to supply a single building with heating and cooling in a multifunctional approach to rainwater management and energy supply [19]. The authors concluded that the heat pump employed in the study was overdimensioned and that the geothermal piping was buried at too shallow depth (35 cm), with detrimental disturbances from seasonal temperature variations, yielding a coefficient of performance (COP) of just 1.8, well below the 2.875 required for satisfactory performance by the 2009 EU Renewable Energy Directive. Nevertheless, the authors further conclude that the combined GSHP-PPS system is expected to perform satisfactorily if designed and dimensioned correctly. They point out the need for building full scale testing of combined SUDS and GSHP.

To address these issues, we propose and demonstrate in full scale, a novel type of energy geostructure that uses a traditional road construction for combining a GSHP with a sustainable urban drainage system, referred to as the "Climate Road". The Climate Road uses the geotechnical gravel structure underlying and stabilizing the road simultaneously as an energy source for the GSHP and as a retarding basin for draining excess surface water through permeable asphalt and roadside drainage grates. 800 m (4 x 200 m loops) of geothermal piping was buried in the roadbed 50 and 100 cm below the pavement surface and connected to an existing GSHP in a nearby kindergarten. We present the construction details for the 50 m full-scale demonstration of the road and present water balance measurements and operational GSHP data for the initial 1135 days of operation. The experimental data serve to validate a computational model of the groundwater and heat transport in the roadbed. Model studies explore the sustainable energy production levels for a 30-year period, as constrained by legislative regulations on brine temperatures for GSHP systems operating in Denmark. We further estimate the effects of rainwater infiltration and seasonal energy storage on sustainable heat production levels. For a more in-depth analysis of rainwater management and retardation with the Climate Road we refer to Andersen et al. [20].

2. Materials and Methods

2.1 Climate Road construction

The full-scale demonstration was carried out in cooperation with the local county in Hedensted, Denmark as part of the Coast to Coast Climate Challenge (C2C-CC) project under the EU Life program. The Climate Road replaces an existing 50 m stretch of road near Hedensted city, scheduled for a complete refurbishment. Moreover, the stretch of road is situated close to a kindergarten which is supplied by an existing GSHP using 1200 m of traditional horizontal collector pipes. The GSHP was disconnected from the existing heat collector and subsequently connected to the geothermal piping in the Climate Road. The location of the full-scale demonstration is shown in Figure 1.

Preprints (www.preprints.org) | NOT PEER-REVIEWED | Posted: 13 May 2022 doi:10.20944/preprints202205.0183.v1

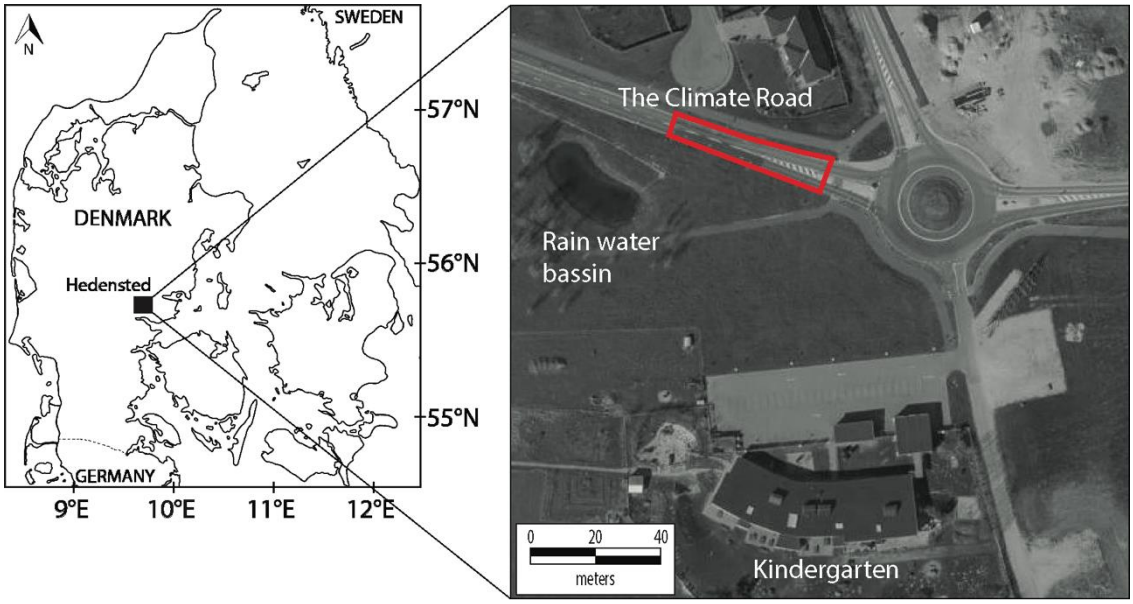

Figure 1. Overview map of the Climate Road. The red polygon indicates the road surface area.

Construction works began on the 18th of September 2017 and the Climate Road was put into operation on the 23rd of March 2018.

Initially, the existing asphalt was removed and excavations for the roadbed commenced. Once completed, the construction pit was lined with a bentonite membrane on the bottom and sides to ensure full hydraulic control of the retarding basin by preventing uncontrolled seepage of groundwater into the roadbed (white textile membrane under pipes in Figure 2).

Preprints (www.preprints.org) | NOT PEER-REVIEWED | Posted: 13 May 2022 doi:10.20944/preprints202205.0183.v1

Figure 2. The construction pit with the bentonite membrane (white geotextile), blue Ø160 mm drainage pipes in the sides, black geothermal piping loops embedded in soft DrænAF gravel with the coarser DrænStabil gravel on top. The kindergarten with the GSHP using the Climate Road as collector, is visible in the top right corner of the picture.

Ø160 mm drainage pipes with slits were then placed on top of the bentonite membrane in small trenches in the sides and ends of the pit, (blue pipes in Figure 2). Two equally spaced 200 m Ø40 mm PE geothermal pipes were then placed on top of the bentonite membrane in a W-configuration and then covered with soft, rounded gravel (black pipes covered with small mounds of soft gravel in Figure 2). With the piping in place, construction of the roadbed commenced. The roadbed material consists of well-sorted gravel from which all fine-grained material has been removed to ensure high porosity. Moreover, the gravel is designed to preserve its structural integrity when fully saturated with water. Information pertaining to the construction materials is listed in Table 1.

Table 1. Technical declarations for the roadbed materials. DS refers to Danish standards that are available in English at https://www.ds.dk/en/about-standards. DrænStabil and DrænAF are registered trademarks of the NCC company.

Properties	Standard/method	DrænStabil®	DrænAF®
Grain size distribution	DS-EN 13285 DS-EN 933-1	G_N D_{50} = 17.0 ±5 D_{15} = 5.3 ±2	G_C85-15 GT_C25/15 D_{50}=3.3±1 D_{15}=2.1±1

Preprints (www.preprints.org) | NOT PEER-REVIEWED | Posted: 13 May 2022 doi:10.20944/preprints202205.0183.v1

Fine grain content	DS-EN 13285/DS-EN 933-1	None	f_2
Shape index	DS-EN 13242/DS-EN 933-4	SI_{20}	-
Degree of crushing	DS-EN 13242/DS-EN 933-5	$C_{50/10}$	$C_{50/30}$
Infiltration velocity (mm/s)	Non-official guideline	>10	15±5
Hydraulic conductivity (mm/s)	DS CEN ISO TC 17892-11	0.5	10±5
Drainable porosity (%)	From reference density	>30	-
Reference density (kg/m³)	DS-EN 13286-5. Vibration with water content=3% ±1	1800	-
Los Angeles index (%)	DS-EN 1097-2	LA_{30}	-
E modulus (MPa)	DS-EN 13286-7	300	-

Two additional 200 m W-configuration geothermal pipes were then placed 50 cm above the bottom of the roadbed in an identical manner to those placed on top of the bentonite membrane. Once the construction of the roadbed was complete, 25 m of the road was paved with permeable asphalt, allowing for vertical water flow directly through the pavement. The remaining 25 m was paved with traditional asphalt with drain grates in the roadsides as shown in Figure 3.

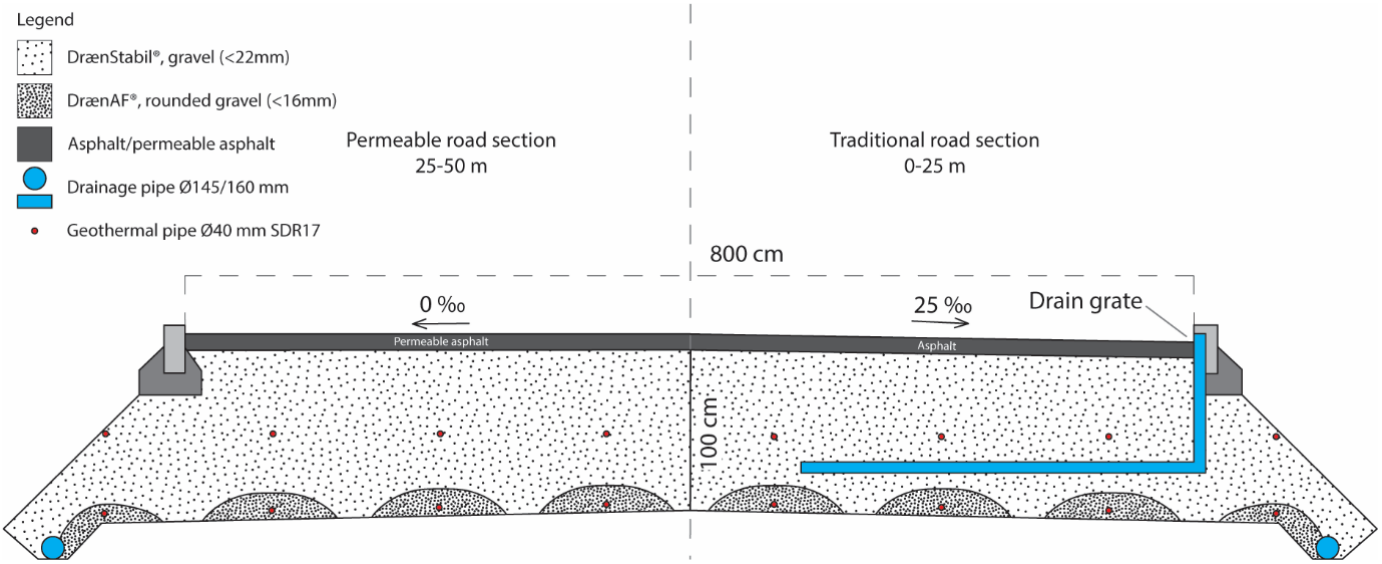

Figure 3. Transect of the road section with permeable and traditional asphalt shown to the left and right of the central vertical dashed line, respectively. Road section interval is relative to the roundabout to the east of the Climate Road as shown on the overview map in Figure 1. The illustration is not to scale.

The permeable asphalt (PermaGAB® from NCC) consists of crushed granite or similar gravel materials with a maximum grain size of 22 mm, mixed with a polymer modified bitumen, yielding a void porosity of 19-23%. A wear layer of PermaSLID®, similar to PermaGAB® in terms of composition and void porosity, but with smaller grains up to 16 mm, is paved on top of the PermaGAB®. The permeability of the permeable asphalt is > 1 cm/s, however, clogging tends to occur over time and soil particles must be removed from the asphalt by a vacuum road sweeper once a year.

The roadbed drains to a nearby basin for experimental reasons. In a commercial application, the roadbed drains to the existing wastewater network through a water brake that restricts discharge even during extreme precipitation events, where excess water is stored and thus delayed in the roadbed instead.

2.2 Temperature model

A temperature model for the road should describe both the transport of heat between the fluid in the geothermal pipes and the surrounding sand and gravel, as well as the larger scale transport throughout the roadbed. Heat transport by conduction and

Preprints (www.preprints.org) | NOT PEER-REVIEWED | Posted: 13 May 2022 doi:10.20944/preprints202205.0183.v1

advection in porous media (the roadbed in this case) is described by the partial differential equation [21]:

$$\rho_s c_s \frac{\partial T_s}{\partial t} = \lambda_s \nabla^2 T_s - \rho_f c_f \nabla \cdot (T_s \mathbf{u}_d), \quad (1)$$

where $\rho_s c_s$ [J/m³/K] is the volumetric heat capacity of the sand and gravel in the roadbed, T_s [K] the temperature in the roadbed, λ_s [W/m/K] the thermal conductivity, $\rho_f c_f$ [J/m³/K] the volumetric heat capacity of the fluid (water) in the pores and $\mathbf{u}_d$ [m/s] is the Darcy velocity vector. Eq. (1) ignores mechanical dispersion of heat and assumes instantaneous thermal equilibrium between the sand/gravel matrix and the flowing groundwater. Moreover, the internal heat production in the porous medium (the source term) is assumed to be zero.

2.2.1 Single pipe model

Each of the four 200 m geothermal pipes is divided into four model segments, yielding 16 pipe segments in total (see Fig. 3). Each segment is modelled as a finite line source under the influence of groundwater flow. We adapt the model developed by Guo et al. [22] for the radial temperature distribution from a single buried borehole heat exchanger (BHE), modelled as a vertical finite line source (see Figure 4a,b)). Groundwater flow is considered to be one-dimensional along the x-axis, so the vector $\mathbf{u}_d$ is reduced to the scalar u_d in the following.

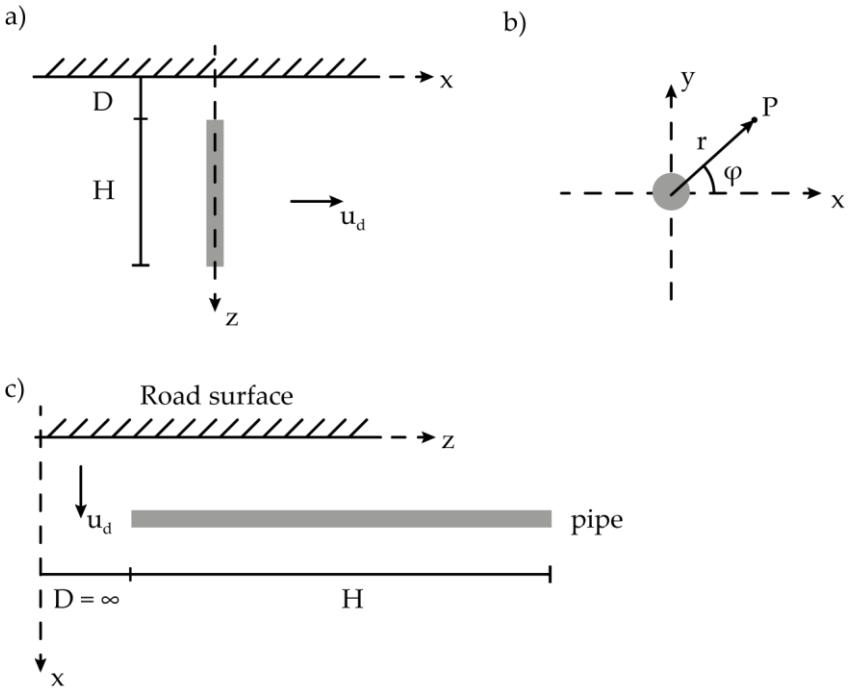

Figure 4: a) Side view of a buried BHE in the model proposed in [20]. b) Top view of the buried BHE. The finite line source model is used to calculate the temperature at a distance r from the borehole. c) In the present case we adapt the model to describe a horizontal pipe section buried in the roadbed.

The temperature averaged over the length of the source is

$$\overline{T}(r, \varphi, t) - T_u = \frac{q}{4\pi\lambda_s} \exp\left(\frac{r \cdot \cos\varphi \cdot U}{2\alpha_s}\right) \cdot \int_{1/\sqrt{4\alpha_s t}}^{\infty} \exp\left(-\frac{U^2}{16\alpha_s{}^2 s^2} - r^2 \cdot s^2\right) \cdot \frac{Fun(Hs, Ds)}{Hs^2} ds, \quad (2)$$

where $\overline{T}(r, \varphi, t)$ [K] is the temperature, T_u [K] is the undisturbed temperature, q [W/m] is the thermal power transferred from the geothermal pipe fluid to the surrounding soil per unit length of pipe, $U = \frac{\rho_f c_f}{\rho_s c_s} \cdot u_d$ [m/s] is the effective thermal transfer velocity, α_s

Preprints (www.preprints.org) | NOT PEER-REVIEWED | Posted: 13 May 2022 doi:10.20944/preprints202205.0183.v1

[m²/s] is the thermal diffusivity, $s = 1/\sqrt{4\alpha_s t}$, H [m] is the length of the pipe and D [m] is the burial depth.
The function under the integral is

$$\mathrm{Fun}(Hs, Ds) = 2 \cdot \mathrm{ierf}(Hs) + 2 \cdot \mathrm{ierf}(Hs + 2Ds) - \mathrm{ierf}(2Hs + 2Ds) - \mathrm{ierf}(2Ds), \quad (3)$$

where ierf is the integral of the error function

$$\mathrm{ierf}(x) = x \cdot \mathrm{erf}(x) - \frac{1}{\sqrt{\pi}}[1 - \exp(-x^2)], \quad (4)$$

The model was initially developed for vertical borehole heat exchangers (BHEs) where burial depth refers to the distance between the top of the BHE and the ground surface (see Fig. 4a). In the present case, the geothermal pipes are placed horizontally with vertical infiltration. Therefore, the distance D effectively becomes infinite (see Fig. 4c). The corresponding limit in Eq. (3) is

$$\lim_{D \to \infty} \mathrm{Fun}(Hs, Ds) = 2 \cdot \mathrm{ierf}(Hs), \quad (5)$$

Disregarding the boundary condition at the road surface for now, Eq. (2) finally becomes

$$\overline{T}(r, \varphi, t) - T_u = \frac{q}{4\pi\lambda_s} \exp\left(\frac{r \cdot \cos\varphi \cdot U}{2\alpha_s}\right) \cdot \int_{1/\sqrt{4\alpha_s t}}^{\infty} \exp\left(-\frac{U^2}{16\alpha_s{}^2 s^2} - r^2 \cdot s^2\right) \cdot \frac{2 \cdot \mathrm{ierf}(Hs)}{Hs^2} ds, \quad (6)$$

At the outer wall of the pipe ($r = r_p$) the temperature averaged over the circumference of the pipe (i.e. the average over the φ coordinate) becomes

$$\overline{T}_p - T_u = \frac{q}{4\pi\lambda_s} \cdot I_0\left(\frac{r_p U}{2\alpha_s}\right) \cdot \int_{1/\sqrt{4\alpha_s t}}^{\infty} \exp\left(-\frac{U^2}{16\alpha_s{}^2 s^2} - r_p^2 s^2\right) \cdot \frac{2 \cdot \mathrm{ierf}(Hs)}{Hs^2} ds, \quad (7)$$

Where I_0 is a modified Bessel function of the first kind. The dimensionless part of Eq. (7) represents the step response, or g function, of the pipe

$$\overline{T}_p - T_u = \frac{q}{4\pi\lambda_s} \cdot g_p(t), \quad (8)$$

similarly, for the temperature in the roadbed (i.e. at $r > r_p$) from Eq. (6)

$$\overline{T}(r, \varphi, t) - T_u = \frac{q}{4\pi\lambda_s} \cdot g_s(r, \varphi, t) \quad (9)$$

2.2.2 Multiple pipe model

The 800 m of geothermal pipe in the Climate Road is modelled as 16 pipe segments as described in Section 2.2.1. For simplicity we assume equal thermal loads q for each segment. In order to enforce a boundary condition at the road surface we use the method of images and include a mirror source for each pipe as indicated in Fig. 5. The average pipe wall temperature response for the 16 pipe segments is

$$g_p^{ave}(t) = \frac{1}{N_p} \sum_{i=1}^{N_p} \left(g_{p,i}(t) + \sum_{j \neq i} g_{s,j}(r_{ij}, \varphi_{ij}, t) + w \sum_{k=1}^{N_p} g_{s,k}(r_{jk}, \varphi_{ik}, t)\right), \quad (10)$$

where Np = 16 is the number of pipes, $g_{p,i}(t)$ is the wall step response for the i'th pipe segment, $g_{s,j}(r_{ij}, \varphi_{ij}, t)$ is the temperature response in the road at the position of the i'th pipe from the j'th pipe, and $g_{s,k}(r_{ik}, \varphi_{ik}, t)$ is the temperature response at the position of the i'th pipe from the k'th mirror source.

The weight w determines the boundary condition at the road surface:

Preprints (www.preprints.org) | NOT PEER-REVIEWED | Posted: 13 May 2022 doi:10.20944/preprints202205.0183.v1

$$\frac{d}{dx}\overline{\Delta T_{rs}} = 0 \text{ for } w = 1, \quad (11)$$

$$\overline{\Delta T_{rs}} = 0 \text{ for } w = -1, \quad (12)$$

For w = 1 the road surface is adiabatic, that is the there is no heat transport across the road surface. Conversely, for w = -1 the road surface is an infinite reservoir ensuring that temperature changes incurred by the GSHP at the road surface are always zero. Intermediate values imply a scaled heat flux at the road surface.

The evolution in the average brine temperature is calculated by temporal superposition of individual temperature responses from variations in the thermal load, the undisturbed temperature profile and the thermal resistance of the geothermal pipe:

$$\overline{T_b}(x,t) = T_u(x,t) + \sum_{i=0}^{N_t-1}(q_{i+1} - q_i)\left[\frac{1}{4\pi\lambda_s} g_p^{ave}(t - t_i) + R_p\right], \quad (13)$$

where N_t is the number of time steps to reach time t and $q_0 = 0$ W/m. The time step is set uniformly to 24 hours in all simulations and all measured data are aggregated accordingly.

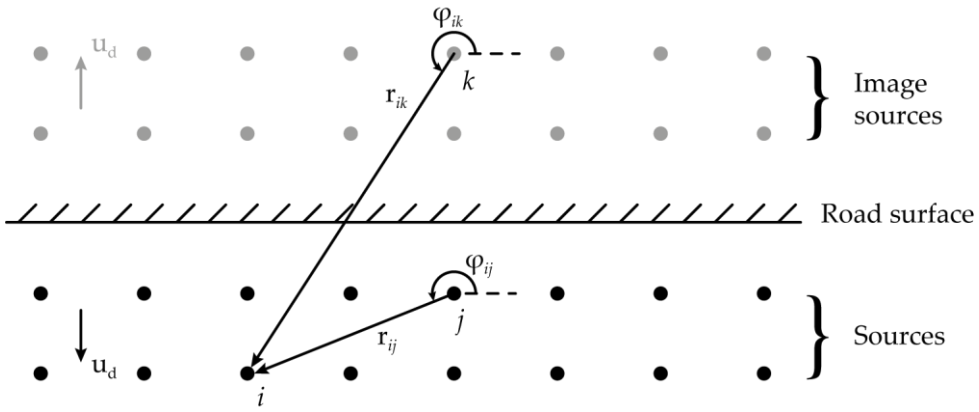

Figure 5. Conceptual illustration of the brine temperature model with the 16 pipe segments embedded in the roadbed. Infiltration into the roadbed is indicated with by the Darcy flow vector u_d. The image sources and Darcy flow vector are shown in grey.

2.2.3 Undisturbed temperatures

As indicated in Eq. (13), the temperature of the roadbed during operation is a calculated by superposition of the seasonal variations in roadbed temperatures and the temperature change incurred by GSHP heat extraction. The undisturbed roadbed temperature $T_u(x,t)$ is estimated by a 1D numerical Crank-Nicolson finite difference discretization of Eq. (1) that adequately captures the propagation of the road surface temperature variations into the subsurface [23]. The scheme is unconditionally stable for any combination of time and space discretisation and is second order accurate in time. The temperature $T_{u,i,j}$ at model node i and timestep j (see Figure 6) is calculated from the preceding timestep according to

$$-0.5KT_{u,i-1,j+1} + (1+K)T_{u,i,j+1} - 0.5KT_{u,i+1,j+1} = 0.5KT_{u,i-1,j} + (1-K)T_{u,i,j} + 0.5KT_{u,i+1,j}, \quad (14)$$

where

$$K = \left(\frac{\alpha_s}{\Delta x} + U\right)\frac{\Delta t}{\Delta x}, \quad (15)$$

Preprints (www.preprints.org) | NOT PEER-REVIEWED | Posted: 13 May 2022 doi:10.20944/preprints202205.0183.v1

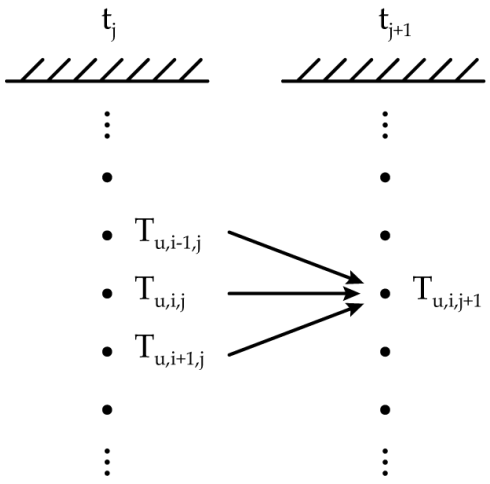

Figure 6: 1D discretization of the subsurface. The temperature at node i is calculated from the temperatures at the node itself as well as both neighbors at the previous timestep

Equation (14) yields a linear system of equations for the temperature at all model nodes at each time step

$$C \cdot \mathbf{T}_{u,j+1} = \mathbf{T}_{u,j}, \tag{16}$$

where the vector $\mathbf{T}_{u,j}$ contains the temperature at all model nodes at timestep j.

The tridiagonal coefficient matrix C is square due to specified temperature boundary conditions at the top and bottom of the model. The matrix is inverted by Gaussian elimination in MATLAB 2021a using the built-in LU decomposition to obtain temperatures $\mathbf{T}_{u,j+1}$

The numerical model extends to 50 m depth and is discretized into 5,000 model layers with a uniform thickness of 1 cm. The time step is 360 seconds. The duration of the simulation is 1135 days for validation using observed temperatures while for long-term projections, a period of 30 years is considered.

The initial temperatures in the roadbed are calculated from the following analytical equation that considers a sinusoidal variation in the surface temperature prior to road construction [26]:

$$T_u(x, t = 0) = 8.5°C + A \cdot \exp\left(-x\sqrt{\frac{\omega}{2\alpha_s}}\right) \cdot \cos\left(\omega t - x\sqrt{\frac{\omega}{2\alpha_s}}\right), \tag{17}$$

where A [K] is the amplitude of surface temperature variation, ω [rad/s] is the angular velocity of the temperature variation.

The temperature boundary condition at the top of the model (x = 0) is set equal to the road surface temperature which is calculated from the empirical equation suggested by [25, Eq. 1] from the wind speed, ambient temperature, relative humidity and solar radiation.

The temperature boundary condition at the bottom of the model is set equal to the undisturbed value $T_u(x = 50\ m, t) = 8.9°C$ as estimated by [26].

When calculating the brine temperature from Eq. (13) we use the simplifying assumption that we can consider the average step response of the 16 pipes. This requires a single value for the background temperature $T_u(x,t)$ As half of the pipes are buried at depth z = 50 cm and half at z = 100 cm we calculate the temperature at both depths using the finite difference model in Eq. (14) and use the arithmetic mean when calculating the brine temperature from Eq. (13).

2.2.4 Model parameters

Preprints (www.preprints.org) | NOT PEER-REVIEWED | Posted: 13 May 2022 doi:10.20944/preprints202205.0183.v1

The model parameters are either table values or fitted from operational data as described in the following. The volumetric heat capacity of the roadbed (mainly sand and gravel) is $\rho_s c_s$ = 2.6 MJ/m³/K, and the volumetric heat capacity of the rainwater permeating the roadbed is $\rho_f c_f$ = 4.186 MJ/m³/K [27].

For the Darcy velocity in Eq. (1) we use 1460 mm/yr corresponding to $u_d = 4.63 \cdot 10^{-8}$ m/s which is the average value estimated from the measured flow rate at the site. Flow measurements are not available for the period from commissioning spanning March 23rd 2018 to June 13th 2018. For this period, we use the average flow measurements from the corresponding periods in 2019 and 2020. The thermal load q in Eq. (13) is measured on the cold side of the heat pump with a Kamstrup energy meter.

The thermal conductivity of the roadbed as well as the pipe thermal resistance is usually estimated from a thermal response test (TRT). No TRT was conducted during the construction of the Climate Road, however in a similar project, an identical road (the Thermoroad) was constructed in 2020 and a TRT was performed on the geothermal pipes. The average fluid temperatures recorded during the TRT are shown in Fig. 7. The interpretation of the TRT data was performed with the numerical model described in [28], yielding an estimate of λ_s = 1.50 W/m/K for the roadbed thermal conductivity and R_p = 0.07 m·K/W for the pipe thermal resistance.

The final model parameter is the weight w for the mirror sources in Eq. (10). w is estimated by minimizing the squared residual between modelled and observed brine temperatures in the period from April 1st 2019 to December 31st 2020. The initial period from March 23rd 2018 to April 1st 2019 is disregarded in the model calibration as the Climate Road was out of operation for some time in this period but also to avoid initial transients that potentially bias estimates of w.

Preprints (www.preprints.org) | NOT PEER-REVIEWED | Posted: 13 May 2022 doi:10.20944/preprints202205.0183.v1

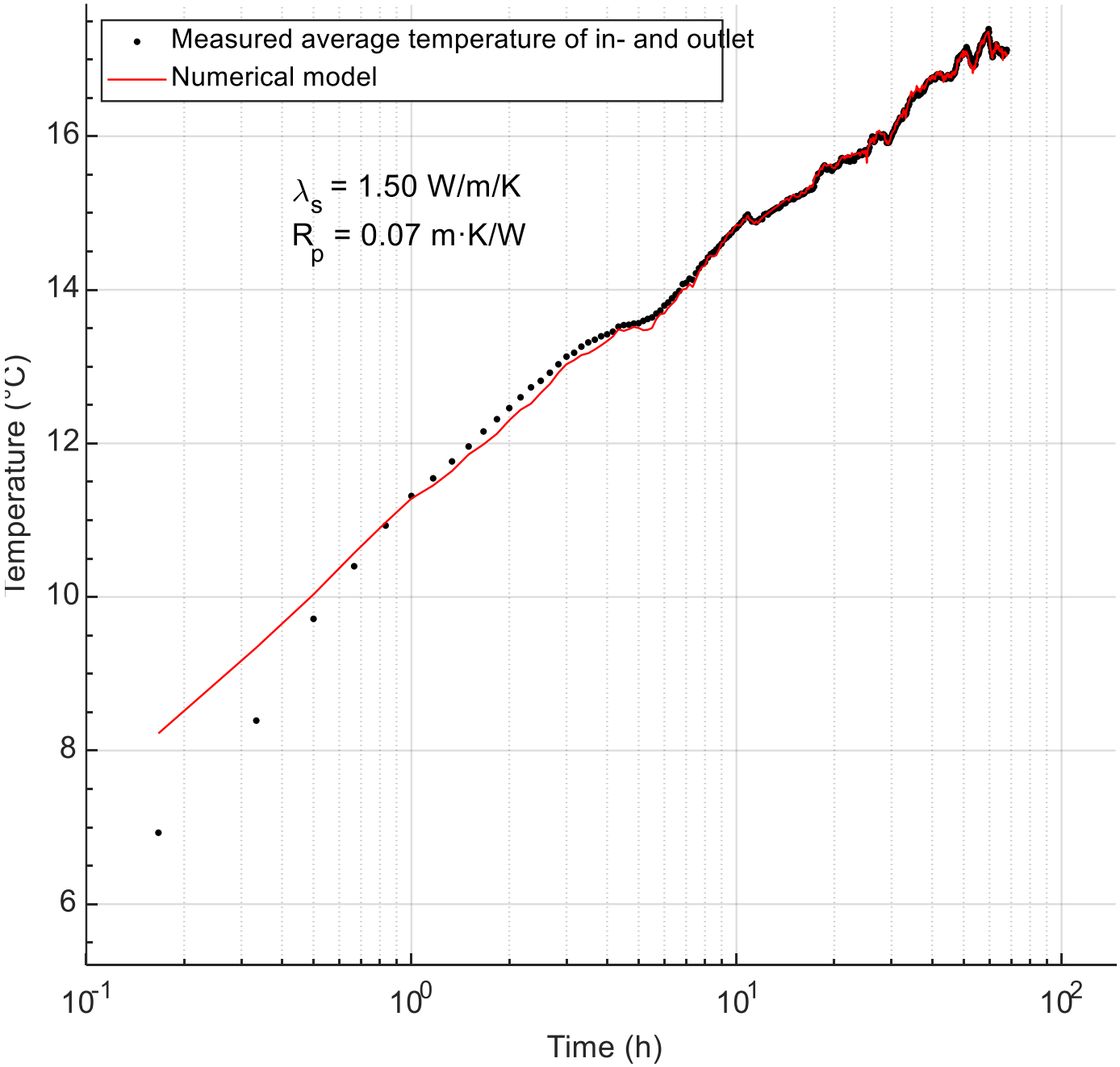

Figure 7. Numerical model interpretation of the TRT of the roadbed geothermal piping from the Thermoroad (duration 48h).

2.3 Instrumentation and measuring data

In the following we present all data relevant to the system performance. This includes weather data for estimating the surface temperature of the road and operational data from the GSHP such as brine temperatures to and from the heat pump, energy extracted from the Climate Road and electricity consumption of the heat pump. Moreover, two flow meters record the water discharge from the two road sections with and without permeable asphalt, respectively. Finally, a Kamstrup energy meter fitted on the cold side of the heat pump, measures the thermal load on the roadbed.

A Davis Vantage Pro2 weather station was used to measure precipitation, air temperature, wind speed and relative humidity. All quantities are aggregated to daily averages. Solar radiation data from the Danish Meteorological Institute (DMI) Bygholm weather station situated 12.5 km from the Climate Road were also used, as the Davis weather station does not measure solar radiation.

Preprints (www.preprints.org) | NOT PEER-REVIEWED | Posted: 13 May 2022 doi:10.20944/preprints202205.0183.v1

Brine fluid temperatures to the heat pump were measured by a Testo 176-T4 datalogger with thermocouple sensors fitted on the exterior of the four geothermal pipes with brine flowing to the heat pump. The average brine fluid temperature was calculated from the temperature decrease across the evaporator which was recorded by the heat pump. Brine temperatures were also measured by the heat pump, however, they are significantly disturbed by the room temperature and are therefore not well-suited for comparison with calculated brine temperatures. Ideally, both the in- and outlet brine temperatures should have been measured with sensors embedded in the geothermal pipes at the manifold, rather than fitted on the exterior pipe wall.

On November 20th 2019, an inspection into a pressure loss issue revealed that one of the 200 m geothermal pipe was leaking brine. Consequently, the leaking pipe was disconnected at the manifold. From a model perspective, this implies recalculation of the g-function at this point in time, as the heat exchanger geometry changes. The corresponding four model segments are removed in the computation of a new g-function and the thermal load is redistributed on the remaining geothermal pipes in the temperature calculation. Consequently, two separate g-functions are computed for the time before and after the disconnection of the leaking pipe, respectively, for predicting the observed brine temperatures.

3. Results

3.1 Weather data and flow measurements

In the following, the weather data and road bed flow meter measurements are presented.

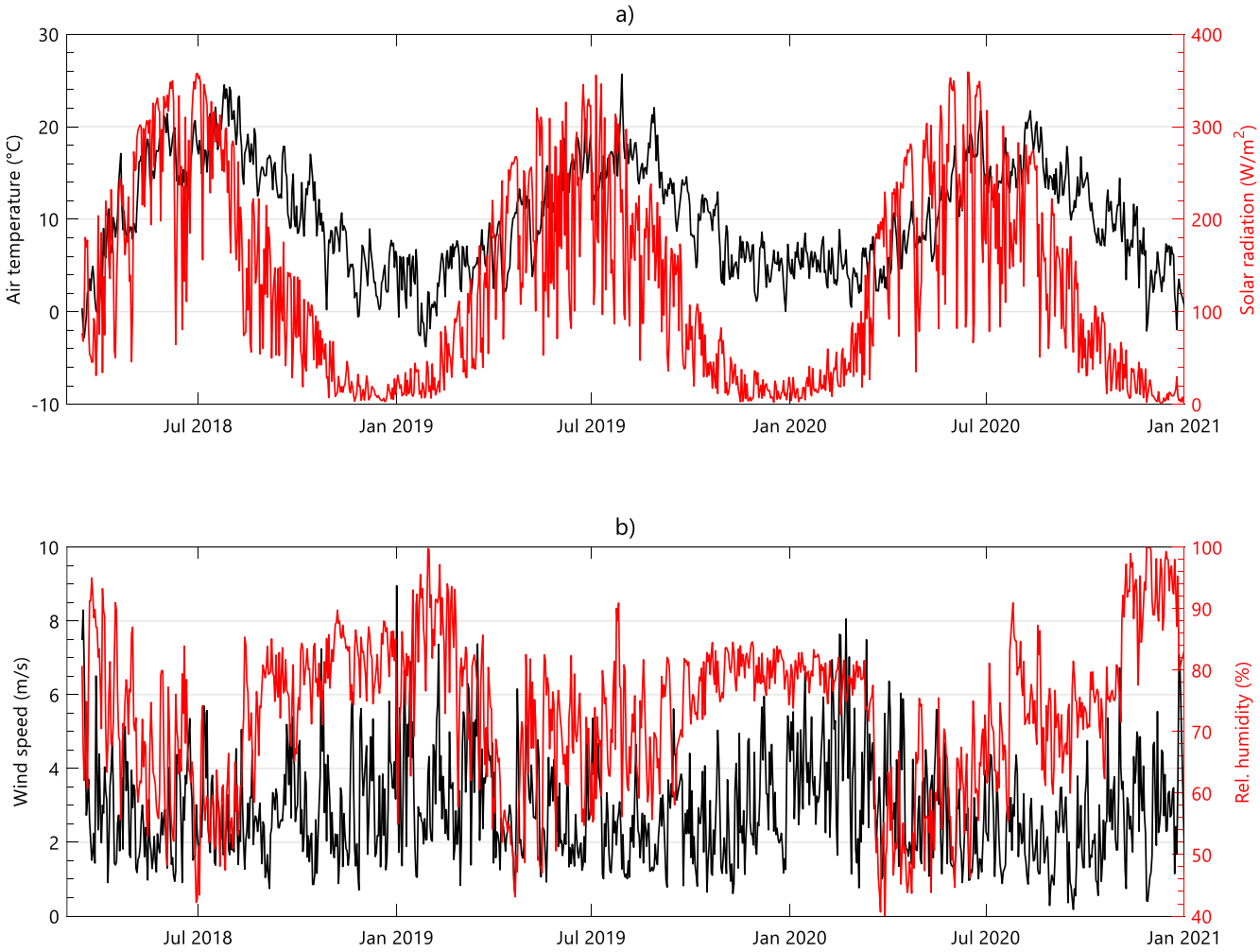

Preprints (www.preprints.org) | NOT PEER-REVIEWED | Posted: 13 May 2022 doi:10.20944/preprints202205.0183.v1

Figure 8. a) Measured daily average air temperature and solar radiation at the Climate Road. b) Wind speed and relative humidity at the Climate Road.

Air temperatures generally reflect seasonal variations in the solar radiation, however, they are phase shifted and somewhat right skewed (Figure 8). Denmark has oceanic climate conditions with daily average air temperature close to zero during the winter months and high relative humidity.

Measured precipitation is compared to corresponding measured monthly Darcy flow rates, estimated by normalizing measured discharge volumes by the 400 m² of road surface (Figure 9).

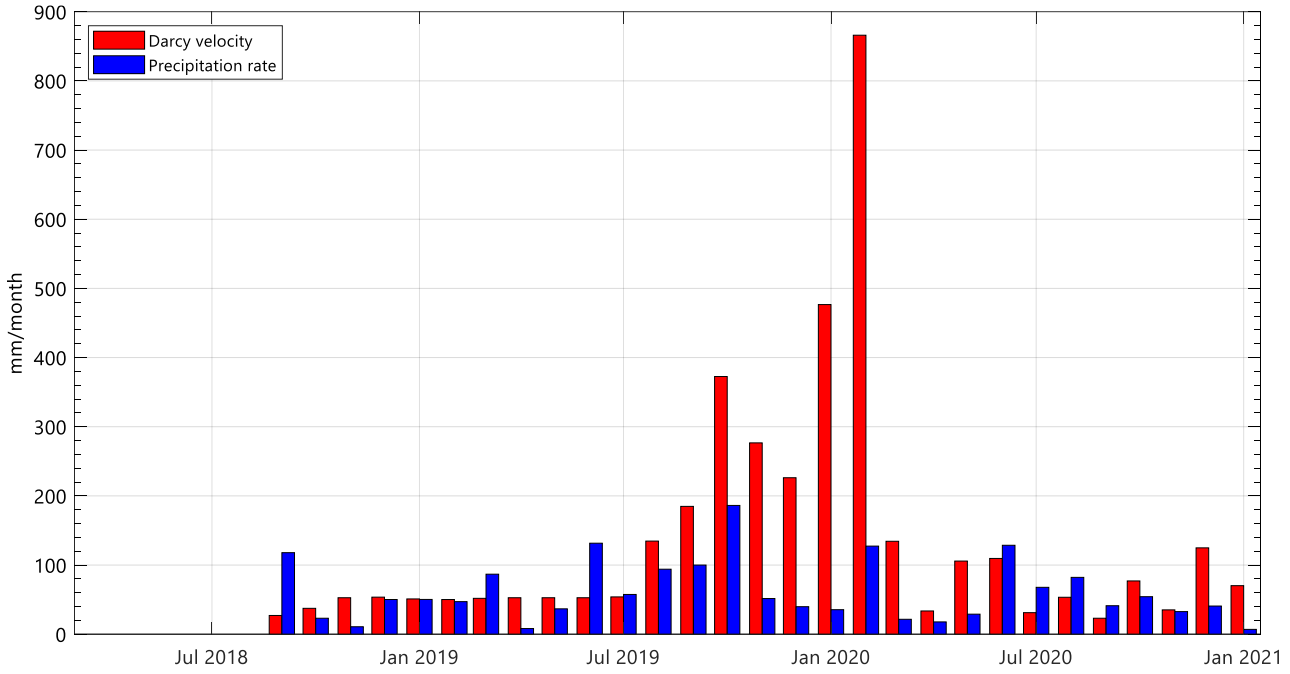

Figure 9. Monthly measured precipitation and estimated Darcy velocity from flow meter measurements.

There is a significant increase in the run-off area that contributes water to the roadbed (i.e. the catchment area) during the winter 2019-2020. The year 2019 was the second wettest on record in Denmark and the field site was visibly waterlogged during the autumn and winter of 2019. As a consequence, the rain water basin to which water from the roadbed was pumped to, overflooded and caused damage to a nearby bicycle and walking path. Several of the wells with instrumentation were flooded at the time, cutting the power to the kindergarten twice.

As the potential evaporation decreases which increases infiltration to the subsurface, the soil eventually becomes fully saturated and run-off coefficients increase significantly in the areas surrounding the Climate Road. The topographic conditions at the study site, directs the increased surface water flow to the Climate Road, greatly increasing the infiltration rates during the winter 2019-2020. The seasonal dynamics in the extent of the catchment area are well-known from studies on rivers and streams [29].

3.2 Brine flow and temperature

Brine flow is generally laminar during GSHP operation as indicated by the computed Reynolds numbers for the test period (Figure 10).

Preprints (www.preprints.org) | NOT PEER-REVIEWED | Posted: 13 May 2022 doi:10.20944/preprints202205.0183.v1

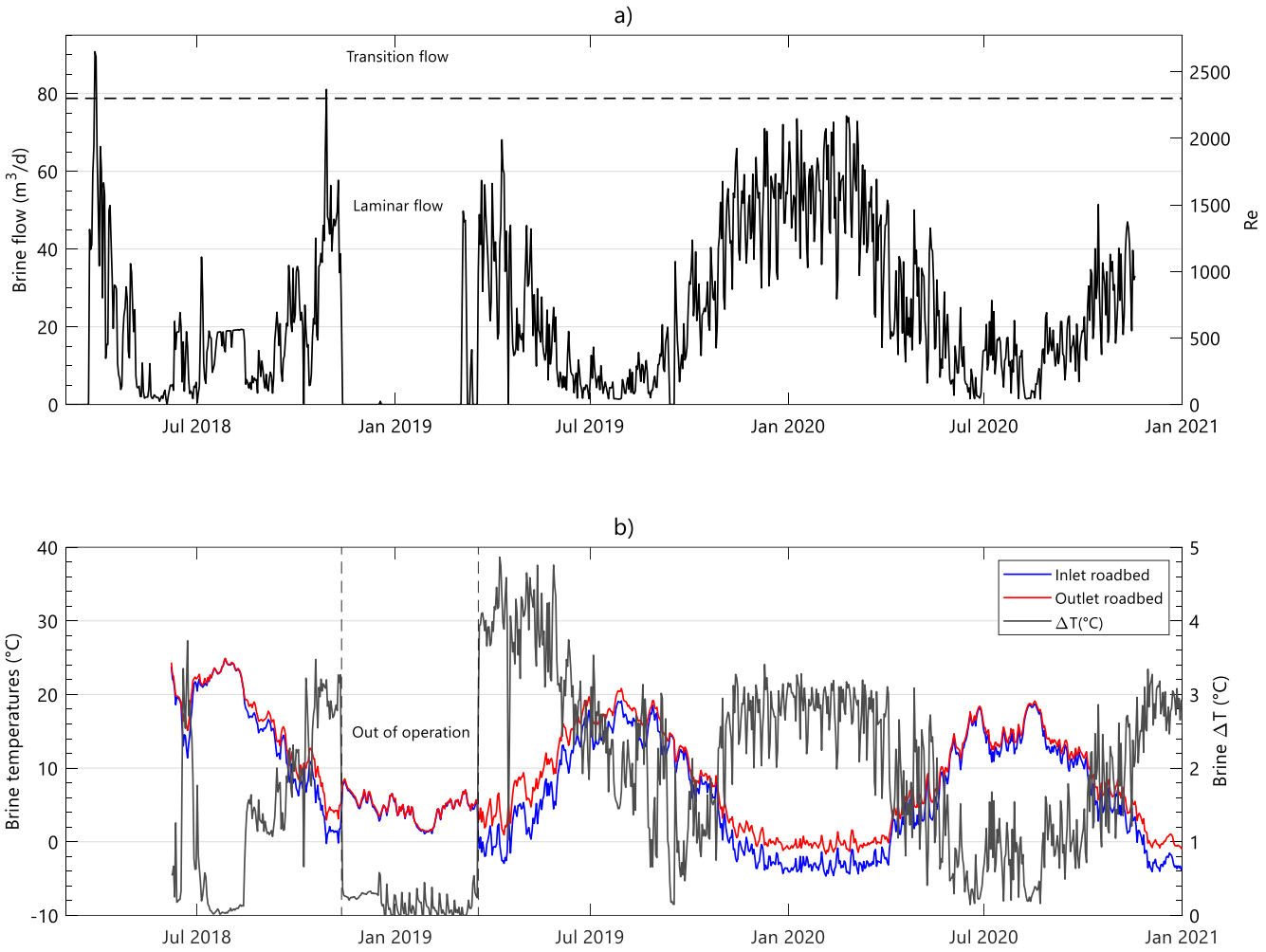

Figure 10. a) Brine flow and Reynolds numbers (Re) during operation. b) In- and outlet temperatures during operation. The hiatus in operation between the 12th of November 2018 and the 19th of March 2019 was due to a fluid pressure issue during which the original collector pipes for the GSHP were used.

To lower the convective thermal resistance of the brine and thereby increase the heat exchange with the ground, flow rates must be maximized to ensure turbulence. However, increasing the flow rate entails increased pumping costs, implying a trade-off between the efficiency of the ground heat exchanger and the cost of brine circulation. The study by Gehlin and Spitler [30] concludes that the pumping costs associated with maintaining fully turbulent or even transition flow exceed the savings from improved heat exchange in the ground. Consequently, they conclude that laminar flow is in fact desirable.

Brine temperatures vary between 10-20°C in the summer and decreases to ca. 0°C during winter as energy extraction from the roadbed increases. The temperature difference across the heat pump evaporator is 0-5°C.

3.3 Energy production and consumption

The energy for domestic hot water and room heating produced by the heat pump amounts to 67.5 and 64.6 MWh in 2019 and 2020, respectively (Figure 11).

Preprints (www.preprints.org) | NOT PEER-REVIEWED | Posted: 13 May 2022 doi:10.20944/preprints202205.0183.v1

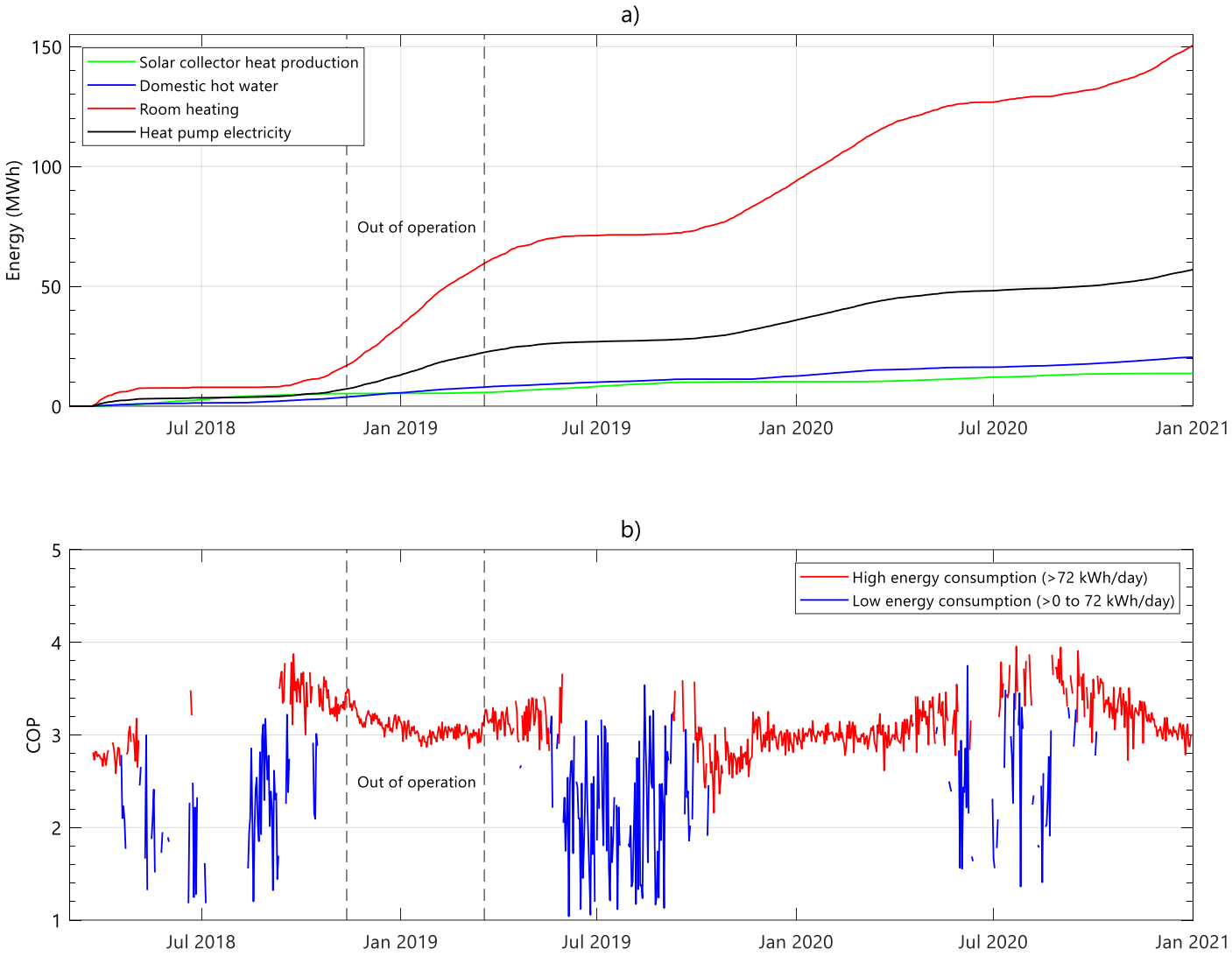

Figure 11. a) Domestic hot water, room heating, electricity consumption by the heat pump and solar collector heat production. b) Daily averages of COP. Out of operation refers to the geothermal piping in the roadbed, not the GSHP, as the original ground collectors was used instead during this period.

Solar collectors increased the heat production by 4.9 MWh and 3.5 MWh in 2019 and 2020, respectively. The average COP is 2.85 in both years, however, in the six coldest months in the winters 2018-2019, 2019-2020 and 2020-2021, the winter seasonal COP (SCOP) is 3.11, 2.94 and 3.15, respectively. The slightly higher SCOP in the winter is attributed to the heat pump being in operation for longer periods of time during the day, thus avoiding frequent starts and stops that are detrimental to performance as illustrated by the blue and red lines in the bottom plot in Figure 11. Depending on the heating system for room conditioning, improvement of the COP is possible by controlling and lowering the supply temperature whenever possible, considering the actual heating demands of the building.

3.4 Temperature model analysis

In the following we present the model validation, followed by a parametric study of infiltration rates and seasonal energy storage, both of which are considered design parameters.

3.4.1 Model validation

Preprints (www.preprints.org) | NOT PEER-REVIEWED | Posted: 13 May 2022 doi:10.20944/preprints202205.0183.v1

The model performance is evaluated by comparing predicted and measured brine temperatures. The corresponding model fit to observed brine temperatures is shown in Figure 12.

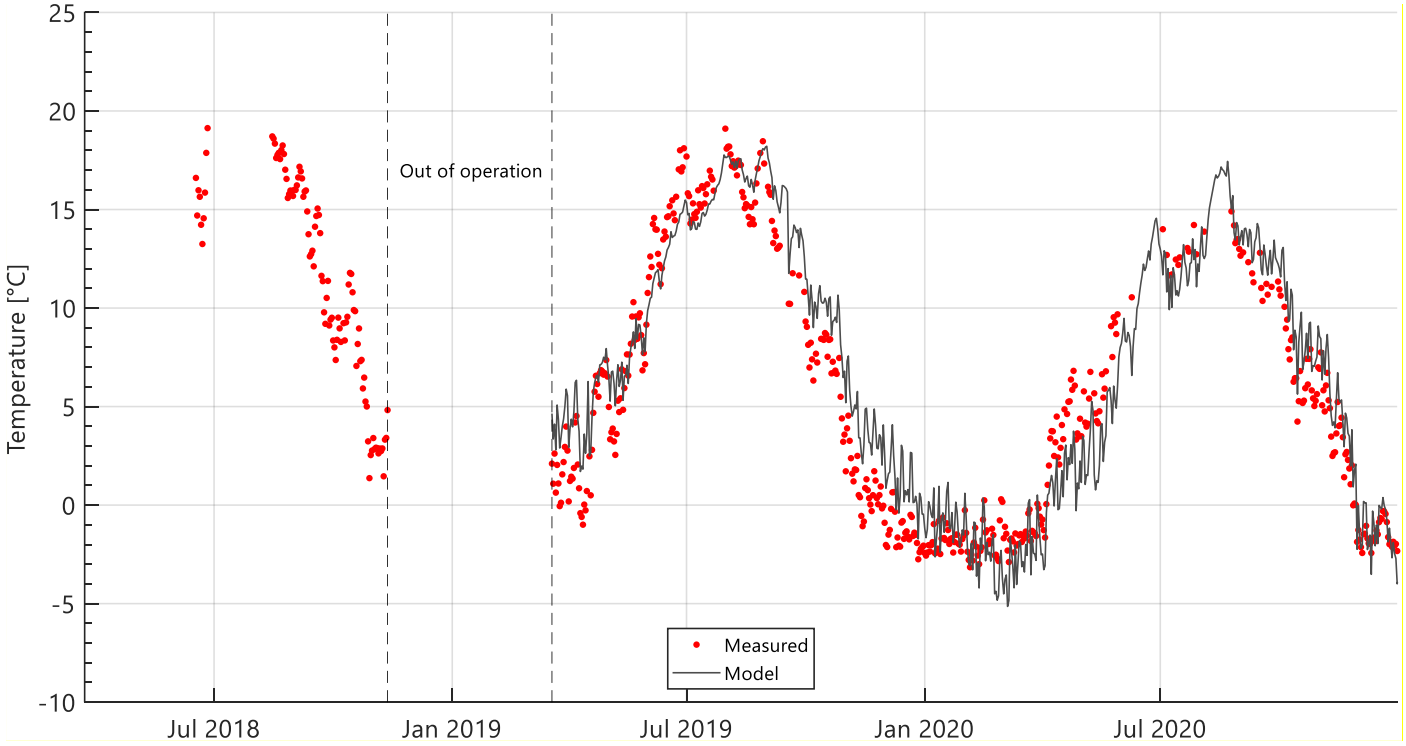

Figure 12. Model predictions of brine temperatures entering the cold side of the heat pump and corresponding measured brine temperatures.

The model predictions correspond fairly well to measured brine temperatures in the period from April 2019 to January 2021.

3.4.2 Prediction of sustainable heat extraction

To make long-term temperature model predictions, the measured thermal load on the roadbed is repeated until the desired simulation time of 30 years is reached. The Climate Road was out of commission from December 2019 to March 2020 and for this period, we use the total heat consumption measured on the condenser side of the heat pump from which we subtract the corresponding electricity consumption to obtain the thermal load on the Climate Road in that period. To estimate sustainable energy extraction rates, the thermal load time series is scaled until the minimum brine temperature supplying the heat pump exceeds -4°C for the full 30-year period.

Assuming a roadbed thermal conductivity of 1.50 W/m/K and an annual infiltration of 1460 mm, the thermal load time series must be reduced by 54% to ensure brine temperatures above -4°C during continued operation for 30 years, corresponding to a total annual heat production of 30.2 MWh including the electricity consumption by the heat pump (Figure 13).

Preprints (www.preprints.org) | NOT PEER-REVIEWED | Posted: 13 May 2022 doi:10.20944/preprints202205.0183.v1

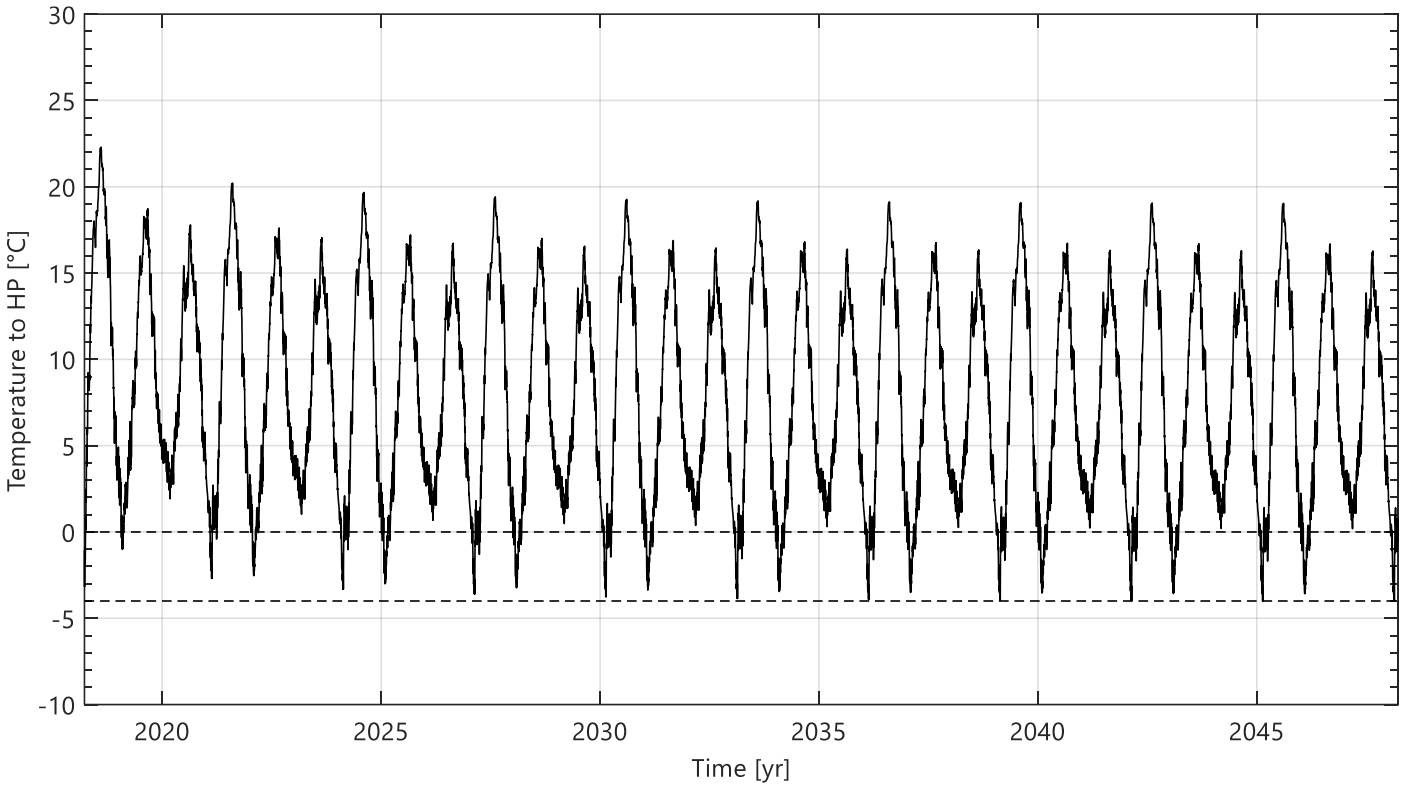

Figure 13. Modelled brine temperatures to the heat pump assuming an annual heat consumption of 30.2 MWh, λ_s = 1.50 W/m/K and u_d = 1460 mm/yr.

The average COP in the 30-year period is assumed to be comparable to current levels around 2.9-3.1 provided that the supply temperature of the heat pump is not altered significantly.

3.4.3 The impact of active infiltration and seasonal energy storage

Infiltration and seasonal energy storage are considered to be design parameters i.e. they can be engineered to a certain degree. A parametric study of the Darcy flow velocity and the seasonal energy storage has therefore been carried out. The infiltration rate is varied between 0 and 2500 mm per year. Additionally, the impact of storing 30% of the annual heating demand is explored. The stored heat can be obtained from passive cooling during summer or from solar collectors or similar energy source. In the analysis we assume the 50 m Climate Road is used as a collective supply for three single family houses, as this represents the most typical and relevant application of the Climate Road.

Approximately 0.52 MWh of total heating (including the contribution from the electricity consumption of the heat pump) can be extracted annually per meter road section in the reference case with zero infiltration and no seasonal energy storage, representing a traditional GSHP system (Figure 14). In this case the 50 m road section is unable to support a consumption of 10 MWh of heating per year. High infiltration rates increase the extractable heat quite substantially, up to 35% for the considered range of infiltration rates and without seasonal energy storage. Given the current field conditions, the amount of extractable heat from the Climate Road is increased by an estimated 17% when compared to the reference case with zero infiltration.

Preprints (www.preprints.org) | NOT PEER-REVIEWED | Posted: 13 May 2022 doi:10.20944/preprints202205.0183.v1

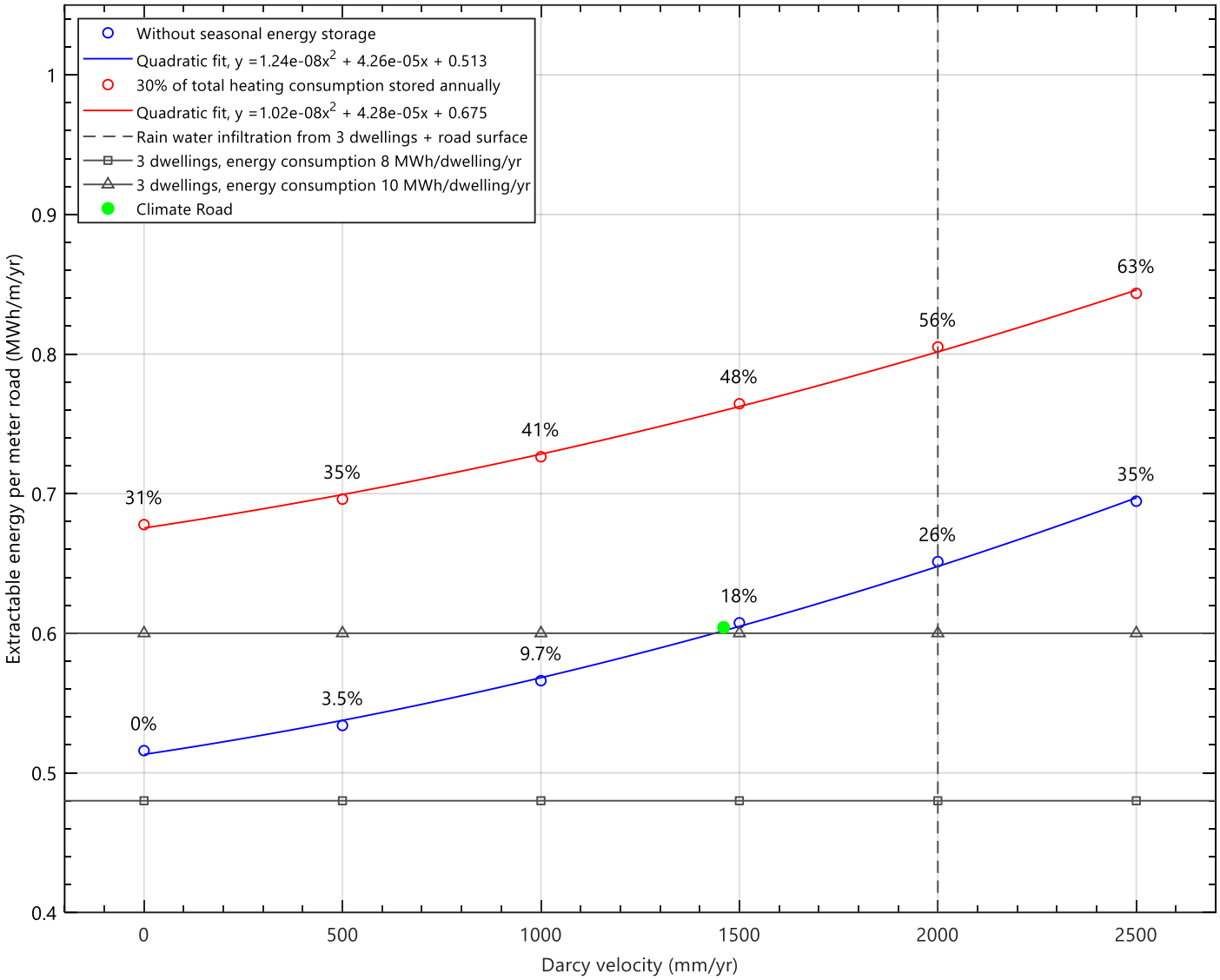

Figure 14. Estimated extractable energy for different infiltration rates and seasonal energy storage. Percentages are relative to the reference case indicated by 0% (zero infiltration, no seasonal energy storage).

In Figure 14, the vertical dashed line indicates the expected Darcy velocity when draining rain water from three dwellings directly to the roadbed (i.e. from house roofs and fortified surfaces). We assume a direct run-off area fraction of 25%. Assuming a plot area of 800 m² per dwelling, the road catchment area is increased by 600 m² in addition to the road surface (400 m²). Based on a total drained area of 1000 m², a conservative estimate of the corresponding Darcy flux in the roadbed is 2000 mm per year, as run-off from non-fortified areas to the Climate Road is not considered. Compared to a traditional GSHP without infiltration, the extractable energy is increased by 26% when 2000 mm of water is infiltrated annually. In this case, the Climate Road is clearly able to supply three dwellings each with an annual heating consumption of 8 MWh. It is also likely that 10 MWh of heating can be supplied to each dwelling annually. Seasonal energy storage of excess heat from the buildings, solar collectors or other energy sources, significantly increases the amount of extractable energy. Storing 30% of the annual heating consumption increases the extractable heat by 56% when infiltrating 2000 mm of rain water per year. In this case, heat supply is guaranteed for an annual heat consumption well above 10 MWh per dwelling. Generally speaking, the increase in extractable energy is proportional to the energy stored.

 doi:10.20944/preprints202205.0183.v1

4. Conclusion

The Climate Road presents an alternative to individual ASHP as it serves as a fully decentralized multifunctional 5th generation district heating and cooling grid. The Climate Road employs GSHPs, that have superior efficiency relative to ASHPs especially on the coldest days in winter. Moreover, the Climate Road voids the need for surface fan heat exchangers that are potentially perceived as both noisy and aesthetically displeasing. Finally, the heat collector thermal piping does not need to be placed on individual plots.

The infiltration of rain water to the roadbed is shown to have a significant, positive effect on the extractable heat. The curvature of the relation between the Darcy velocity and extractable heat is slightly reduced when utilizing seasonal storage, suggesting a small, negative influence of groundwater flow on the possibilities for thermal balancing of the grid. Nevertheless, and quite interestingly, the parametric study suggests that the presence of groundwater flow from rainwater infiltration at the considered rates, does not seem to significantly hamper the possibilities for seasonal energy storage, which would otherwise have been a concern as flowing water tends to reduce soil temperature differences relative to the ambient temperature. While rain water infiltration to the roadbed increases the extractable energy and the security of supply, the addition of seasonal energy storage ensures that the heating demand from three dwellings can be fully supplied by the Climate Road. Active cooling is most likely required to provide reasonable performance, if cooling needs are considered as well, since brine temperatures are quite high during summer. The unwanted building heat is stored in the roadbed from summer to winter, presenting an excellent opportunity for seasonal energy storage. Thermal grids benefit strongly from seasonal energy storage and allows for the exchange of contrasting thermal demands and for utilizing waste heat, creating synergy and economies of scope. Finally, using the subsurface as a thermal storage ensures relatively high source temperatures year-round, most importantly during the coldest days of winter. This way, the likelihood of peaks in electricity consumption and power grid blackouts from low-performing air-source heat pumps is effectively reduced.

The present study targets

a proof of technology, not a proof of business. There are some obvious savings to the initial investment that are made possible by the Climate Road as the roadbed is constructed in any case. However, typically a traditional roadbed is just 50 cm deep. This is too shallow for rain water management and heat production. An additional 50 cm must be excavated, to ensure that seasonal surface temperature variations do not significantly erode the thermal performance during winter. These additional costs must be considered in a business case study of the Climate Road. There are also some pivotal decisions to make, regarding models for ownership and operation. The heating supply benefits significantly from water infiltration, in terms of the upfront investment and the variable costs of operation, sparking a discussion on how to distribute the initial investment and variable costs between the district heating company and the wastewater utility.

Author Contributions: Conceptualization, S.E.P., T.R.A.; methodology, S.E.P., T.R.A., K.W.T..; software, S.E.P., K.W.T.; validation, S.E.P., K.W.T.; formal analysis, S.E.P., K.W.T..; investigation, T.R.A., S.E.P.; resources, T.R.A., S.E.P; data curation, K.W.T, S.E.P, T.R.A.; writing—original draft preparation, S.E.P.; writing—review and editing, S.E.P., K.W.T., T.R.A.; visualization, S.E.P..; supervision, T.R.A.; project administration, T.R.A.; funding acquisition, T.R.A. All authors have read and agreed to the published version of the manuscript.

Funding: Please add: This research project was funded by EU LIFE, grant number LIFE15 IPC/DK/000006-C2C CC.

Data Availability Statement: Not applicable.

Acknowledgments: The authors thank the municipality of Hedensted for their assistance and collaboration on constructing the Climate Road. We also kindly thank Kirsten Landkildehus Thomsen for her careful field and laboratory work. Finally, the authors would like to thank the journal reviewers whose constructive and relevant comments significantly improved the paper.

Conflicts of Interest: The authors declare no conflict of interest. The funders had no role in the design of the study; in the collection, analyses, or interpretation of data; in the writing of the manuscript, or in the decision to publish the results.

References

1. IPCC, Climate Change 2022: Impacts, Adaptation, and Vulnerability. Contribution of Working Group II to the Sixth Assessment Report of the Intergovernmental Panel on Climate Change [H.-O. Pörtner, D.C. Roberts, M. Tignor, E.S. Poloczanska, K. Mintenbeck, A. Alegría, M. Craig, S. Langsdorf, S. Löschke, V. Möller, A. Okem, B. Rama (eds.)]. Cambridge University Press. In Press, **2022**.
2. Vargas, C.A., Caracciolo, L. & Ball, P.J. Geothermal energy as a means to decarbonize the energy mix of megacities. Commun. Earth Environ 3, 66, **2022**, https://doi.org/10.1038/s43247-022-00386-w
3. European Commission. An EU strategy on heating and cooling. Brussels, Belgium: European Commission (EC), **2016**.
4. Lund, J. W., Toth, A. N. Direct Utilization of Geothermal Energy 2020 Worldwide Review, Published in Proceedings of the World Geothermal Congress 2020; Reykjavik, Iceland, April 26 – May 2, **2020**.
5. Reese, S., editor. Advances in ground source heat pump systems, Woodhead Publishing Series in Energy: Number 100: Duxford, United Kingdom, **2016**, pp. 1-452.
6. Staffell, I., Brett, D., Brandon, N., Hawkes, A. A review of domestic heat pumps. Energy and Environmental Science **2012**, 5, pp. 9291-9306.
7. Gabrielli, L., Bottarelli, M. Economic performance of ground source heat pump: does it pay off? In Proceedings of the World Renewable Energy Congress; Linköping, Sweden, 08-13 May **2011**, http//dx.doi.org/10.3384/ecp110571329.
8. Poulsen, S.E.; Alberdi-Pagola, M.; Cerra, D.; Magrini, A. An Experimental and Numerical Case Study of Passive Building Cooling with Foundation Pile Heat Exchangers in Denmark. Energies **2019**, 12, 2697. https://doi.org/10.3390/en12142697
9. Pellegrini, M.; Bianchini, A. The Innovative Concept of Cold District Heating Networks: A Literature Review. Energies **2018**, 11, 236. https://doi.org/10.3390/en11010236.
10. Buffa, S., Cozzini, M., D'Antoni, M., Baratieri, M., Fedrizzi, R. 5th generation district heating and cooling systems: A review of existing cases in Europe. Renewable and Sustainable Energy Reviews **2019**, 104, 504-522.
11. Lindhe, J., Javed, S., Johansson, D., Bagge, H., A review of the current status and development of 5GDHC and characterization of a novel shared energy system, Science and Technology for the Built Environment, **2022**, DOI: 10.1080/23744731.2022.2057111
12. European Commission. Communication from the commission to the european parliament, the council, the european economic and social committee and the committee of the regions. Powering a climate-neutral economy: An EU Strategy for Energy System Integration. COM(**2020**) 299 final.
13. D'Odorico, P., Davis, K. F., Rosa, L., Carr, J. A., Chiarelli, D., Dell'Angelo, J., et al. The global food-energy-water nexus. Reviews of Geophysics **2018**, 56, 456– 531. https://doi.org/10.1029/2017RG000591.
14. Price, S. J., Terrington, R. L., Busby, J., Bricker, S., Berry, T. 3D ground-use optimisation for sustainable urban development planning: A case-study from Earls Court, London, UK. Tunnelling and Underground Space Technology **2018**, 81, pp. 144–164.
15. Cerra, D., Alberdi-Pagola, M., Andersen, T. R., Tordrup, K. W., & Poulsen, S. E. Feasibility study of collective heating and cooling based on foundation pile heat exchangers in Vejle (Denmark). Quarterly Journal of Engineering Geology and Hydrogeology **2021**, 54, qjegh2020-114. https://doi.org/10.1144/qjegh2020-114.
16. Brandl, H. Energy foundations and other thermo active ground structures. Géotechnique **2006**, 56, pp. 81 – 122.
17. Laloui L., Loria A. F. R. Analysis and design of energy geostructures, 1st ed.; Academic Press Elsevier, NA, NA, **2019**, ISBN: 9780128206232.
18. Loveridge, F. McCartney, J. S., Narsilio, G. A., Sanchez, M. Energy geostructures: A review of analysis approaches, in situ testing and model scale experiments, Geomechanics for Energy and the Environment **2020**, 22, pp. 1-30.
19. Charlesworth, S.M., Faraj-Llyod, A.S., Coupe, S.J. Renewable energy combined with sustainable drainage: Ground source heat and pervious paving, Renewable and Sustainable Energy Reviews **2017**, 68, 912–919.
20. Andersen, T. R., Poulsen, S. E., Tordrup, K. W., The Climate Road—A Multifunctional Full-Scale Demonstration Road That Prevents Flooding and Produces Green Energy, Water 2022, 14, 666. https://doi.org/10.3390/w14040666
21. Domenico, P.A. and Schwartz, F.W., Physical and Chemical Hydrogeology. 2nd Edition, John Wiley & Sons Inc., New York, **1998**.
22. Guo, Y., Hu, X., Banks, J., Liu, W.V., Considering buried depth in the moving finite line source model for vertical borehole heat exchangers - A new solution, Energy and Buildings **2020**, 214, pp. 1-15.
23. Crank, J., Nicolson, P. A practical method for numerical evaluation of solutions of partial differential equations of the heat conduction type. Proc. Camb. Phil. Soc. **1947,** 43, 50–67. doi:10.1017/S0305004100023197.
24. Fowler, C.M.R. The Solid Earth, An Introduction to Global Geophysics; Cambridge University Press: Cambridge, UK, **2005**, pp. 230–231, p. 685.
25. Khan, Z. H., Islam, M. R., Tarefdera, R. A. Determining asphalt surface temperature using weather parameters. Journal of Traffic and Transportation Engineering (English Edition) **2019**, 6, pp. 577-588.

 doi:10.20944/preprints202205.0183.v1

26. Møller, I., Balling, N., Ditlefsen, C. Shallow subsurface thermal structure onshore Denmark: temperature, thermal conductivity and heat flow. Bulletin of the Geological Society of Denmark **2019**, 67, pp. 29–52.
27. VDI (Verein Deutscher Ingenieure) Thermische Nutzung des Untergrundes: Grundlagen, Genehmigungen, Umweltaspekte. Richtlinie 4640, Blatt 1, 33 pp. Dusseldorf: Verein Deutscher Ingenieure. **2010**.
28. Poulsen, S. E., Alberdi Pagola, M. Interpretation of ongoing thermal response tests of vertical (BHE) borehole heat exchangers with predictive uncertainty based stopping criterion. Energy, **2015**, 88, pp. 157-167. https://doi.org/10.1016/j.energy.2015.03.133
29. Latron, J., Gallart, F. Seasonal dynamics of runoff-contributing areas in a small Mediterranean research catchment (Vallcebre, Eastern Pyrenees). Journal of Hydrology **2007**, 335, pp. 194-206, https://doi.org/10.1016/j.jhydrol.2006.11.012.
30. Gehlin, E. A., Spitler, J. D. Effects of Ground Heat Exchanger Design Flow Velocities on System Performance of Ground Source Heat Pump Systems in Cold Climates, ASHRAE Winter Meeting, Chicago, Illinois, January 24-28, **2015**.